Supporting information for:

Electrothermal patches driving the transdermal delivery of insulin

Quentin Pagneux,[†,‡,§] Ran Ye,[¶,§] Chengnan Li,[†] Alexandre Barras,[†] Nathalie Hennuyer,[‡] Bart Staels,[‡] Darwin Caina,[¶] Jonathan Israel Avila Osses,[¶] Amar Abderrahmani,[†] Valérie Plaisance,[†] Valérie Pawlowski,[†] Rabah Boukherroub,[†] Sorin Melinte,[*,¶] and Sabine Szunerits[*,†]

[†]*University of Lille, CNRS, Centrale Lille, ISEN, Université de Valenciennes, UMR 8520 - IEMN, F-59000 Lille, France*

[‡]*University of Lille, Inserm, CHU Lille, Institut Pasteur de Lille, U1011 - EGID, F-59000 Lille, France*

[¶]*Institute of Information and communication Technologies, Electronics and Applied Mathematics, Université catholique de Louvain, 1348 Louvain-la-Neuve, Belgium*

[§]*contributed equally to this work*

E-mail: sorin.melinte@uclouvain.be; sabine.szunerits@univ-lille.fr

Contents

Materials and methods

Figure S1 includes scanning electron microscopy (SEM) images of structures of different gold nanoholes arrays deposited on Kapton formed by colloidal lithography by changing the etching time and an optical image of the active side of a disc type unpatterned device. A typical SEM image and a Raman spectrum of reduced graphene oxide (rGO) coated gold nanoholey electrothermal patches are also presented.
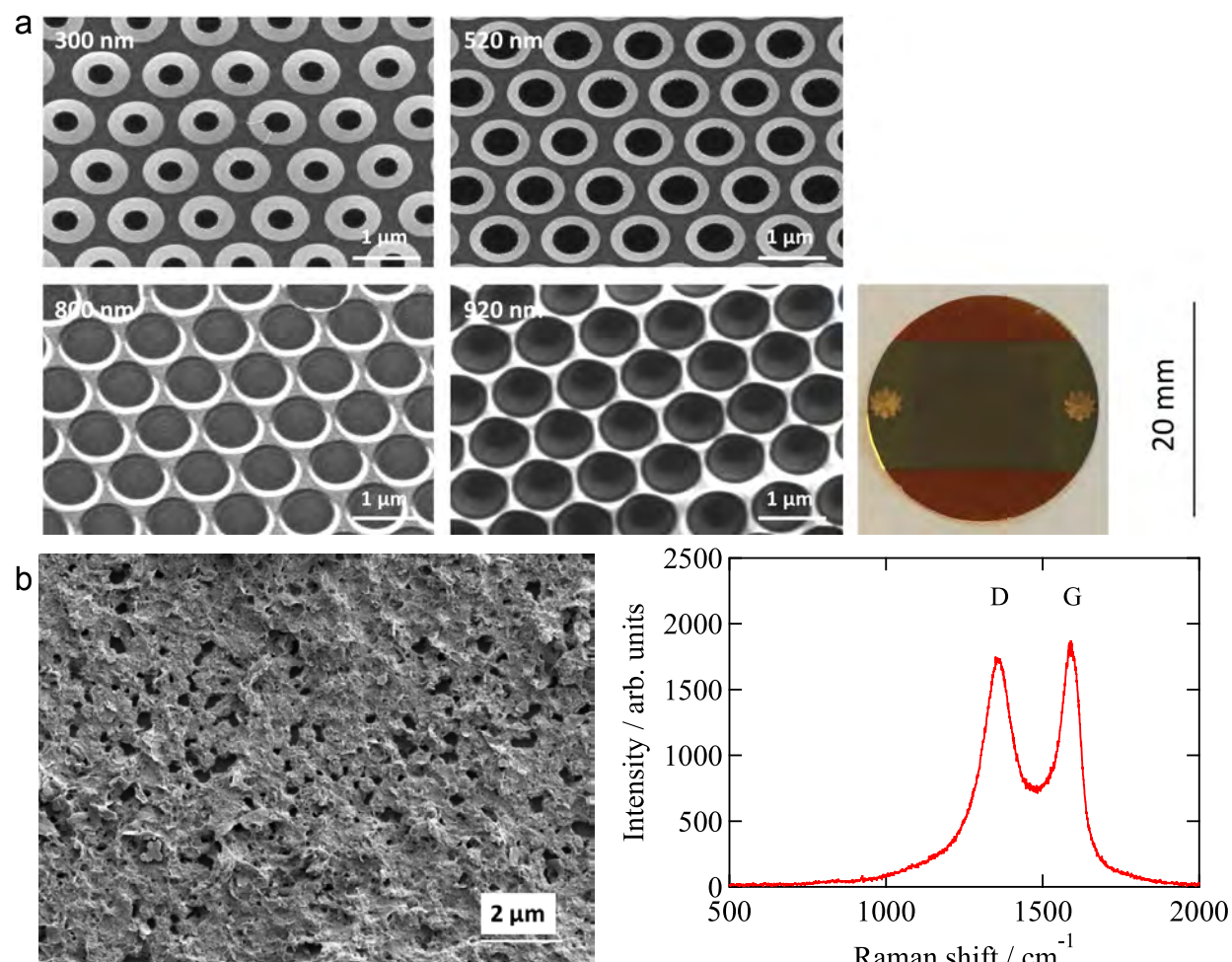
Figure S1: (a) SEM images of K/Au NHs devices and optical image of the heater design in the skin patches. (b) SEM and Raman analysis of K/Au NHs-rGO devices.

In Table S1 we present different structural parameters of the fabricated devices. The etching time corresponds to a power of 30 W, 30 sccm O_2, 1 sccm SF_6, $T = 15\,^{\circ}\mathrm{C}$ (sample), and DC bias of 163 V.

Table S1: Etching times, hole diameters, format and electrical resistance for the designed electrothermal patches.

	Etching time	Hole diameter	Format	Resistance ($\Omega/\square$)
K/Au NHs300	17 min 30 s	300 ± 30 nm	Disk and Rectangle	3.2 ± 0.2
K/Au NHs500	15 min 10 s	520 ± 30 nm	Disk and Rectangle	4.2 ± 0.2
K/Au NHs800	7 min	800 ± 30 nm	Disk and Rectangle	8.4 ± 0.2
K/Au NHs900	5 min	920 ± 30 nm	Disk and Rectangle	22.3 ± 1.3
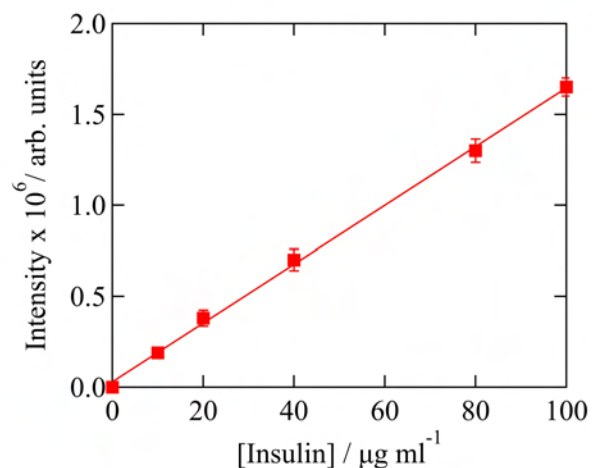
Figure S2: Calibration curve of insulin determined by HPLC and linear fit to the data.

The Franz cell used for transdermal insulin delivery experiments comprises two parts. The bottom part consists of a carved disc of 35 mm in outer diameter (7 mm in thickness) and of 19.5 mm inner diameter (6 mm in thickness). The piece is pierced at its center with a hole of 1 cm in diameter. Two 6 mm thick sculpted zones of 13.0×4.7 mm^2 and 11.0×3.9 mm^2 are accommodated into the disc to facilitate the electrical connections to instrumentation.
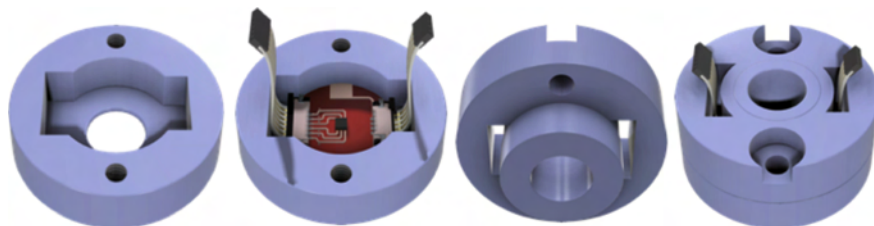
Figure S3: Schematics of the Franz cell used for transdermal insulin delivery experiments.

At the outer part, there are two tapped holes having 3.3 mm in diameter for connection to the top part. The top part (35 mm in diameter, 9 mm in thickness) continues with a cylinder of 19.5 mm in diameter, 6 mm in thickness. Two exits having the same dimensions as that of the sculped zones in the bottom part are carved for accessing the electrical contacts of the patch. Two 4 mm in diameter holes are drilled on the outer part for accommodating the fixation screws.
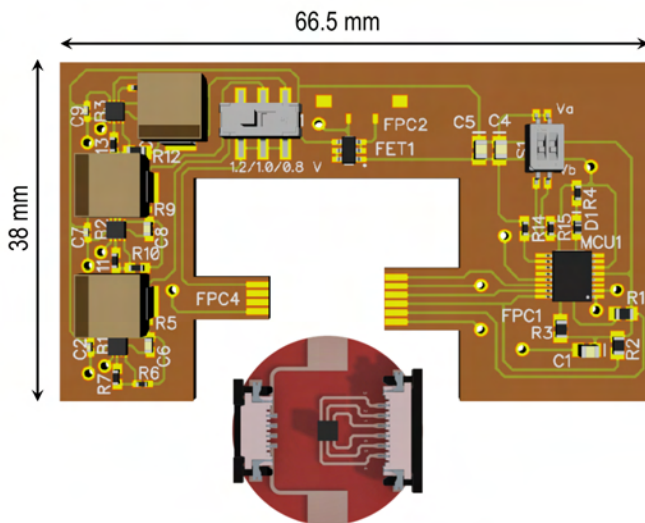
Figure S4: Schematics of the flexible printed circuit board to control the electrothermal skin patches.

We used standard Kapton films (thickness of 50 microns) for the integration of electrothermal skin patches, that can be powered via 2.4 V flexible, rechargeable Li-ion batteries. Temperature recording was verified by a thermal camera to ensure that the patch induces a homogenous distribution of the temperature across the active surface without the presence of any hot spots.

Numerical calculations

Joule heating calculations of a Kapton® tape covered with a gold thin film heated by an applied electrical current are carried out numerically, considering a periodic array of nano-sized holes patterned in the gold layer, and obtaining thus their overall effect on the thermal and electric conductivities of the system. Effective parameters are obtained and then used in a macroscopic calculation, revealing the dependence of maximum attainable temperature and electrical current on the hole size. The highest temperatures are obtained without holes, but in that case, the electrical current increases to several amperes due to the low resistance of the gold thin film. Then, suitable hole diameters and film thicknesses are analysed such that temperatures <50 °C and electrical currents <1 A are expected in heating gold thin films of ∼1 cm × 1 cm at applied biases of ∼1.5 V.

The propagation of heat with a Joule heating source $\boldsymbol{j} \cdot \boldsymbol{E}$ is modelled by the equation:[S1]

$$\rho \bar{c} \frac{\partial T}{\partial t} = \nabla \cdot \kappa \nabla T + \boldsymbol{j} \cdot \boldsymbol{E}, \tag{1}$$

where $\bar{c}$ is the unit mass heat capacity, ρ the mass density, κ the thermal conductivity, T the temperature, t the time, $\boldsymbol{j}$ the electric current density and $\boldsymbol{E}$ the electric field. Heat sinks at temperature T_{ref} can also be included in the volume or as boundary conditions.

The electric current density and the electric field are obtained from the electric potential ϕ whose distribution is ruled by the equation $\nabla \cdot \sigma \boldsymbol{E} = 0$ with suitable boundary conditions. The electric field is given by $\boldsymbol{E} = -\nabla \phi$ and $\boldsymbol{j} = \sigma \boldsymbol{E}$, with σ being the electrical conductivity of the material. The current complies with $\boldsymbol{j} \cdot \hat{n} = 0$ at non-conducting boundaries. No radiative heat loss was considered.

Simplified periodic geometry

First, we consider the properties of the system at the scale comparable to the diameter of holes patterned in the heating gold thin film, with periodic boundary conditions. The

domain considered is a rectangular vertical section of the system of lateral span $0 < x < L$ and $0 < y < w$, with $L = 3.92 \times 10^{-6}$ m and $w = 3.3948 \times 10^{-6}$ m. Given the thickness of the Kapton as $t_K = 1.25 \times 10^{-4}$ m, the thickness of the gold film $t_h = 40 \times 10^{-9}$ m, the total height of the vertical section is $t_K + t_h$. Triangular arrays of holes of diameters from 50 to 900 nm are considered for the gold thin film, with a separation $a = 980$ nm. Some details of the discretization used in the numerical computations can be seen in Fig. S5 and Fig. S6.
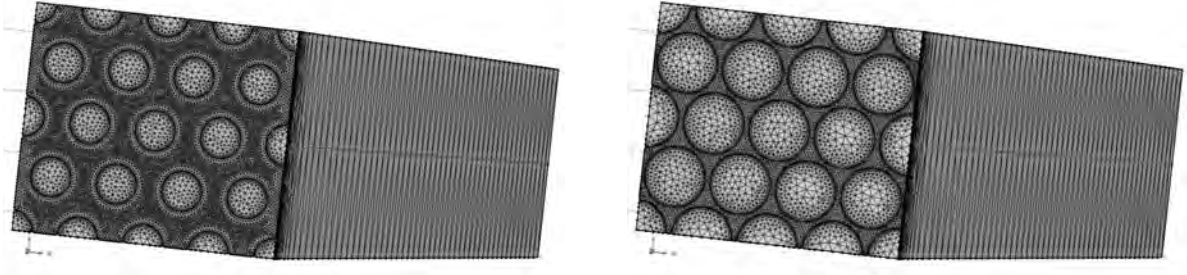
Figure S5: Left: Discretization used for the system with 600 nm diameter holes. Right: Discretization used for the system with 900 nm diameter holes.
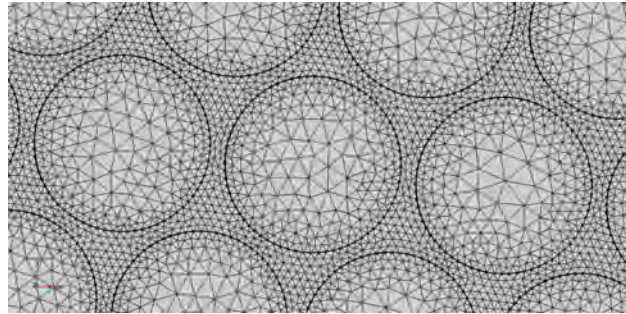
Figure S6: Zoom on the mesh generation for the system with 900 nm diameter holes.

Boundary conditions

Periodic boundary conditions for the temperature are considered at x and y faces, namely: $T(x = 0) = T(x = L)$ and $T(y = 0) = T(y = w)$. Flux boundary conditions are considered at the top and bottom faces, $\kappa \hat{n} \cdot \nabla T = -h(T - T_{ref})$, with $h = 250$ W/(m^{2}K) and $T_{ref} = 293.15$ K, where $\hat{n}$ is the exterior unitary normal to the boundary.

For the electric potential, periodic boundary conditions are established between the y faces,

$\phi(y = 0) = \phi(y = w)$. The ground is at $x = L$ and a voltage $\delta V_a = V_a \cdot L/1$ cm is applied at $x = 0$, where V_a is the voltage applied in the 1 cm macroscopic sample.

Physical parameters

Temperature dependent electrical conductivity, thermal conductivity and constant specific heat were considered for gold, and temperature dependent specific heat and thermal conductivity were considered for Kapton, with fits in the range 250 - 400 K from data obtained from literature,[S2–S5] namely:

$$\rho_{eAu}/[10^{-8}\Omega \text{ m}] = -2.53 \times 10^{-1} \pm 2 \times 10^{-2} + (8.37 \times 10^{-3} \pm 6 \times 10^{-5})T/[K]$$

$$k_{Au}/[\text{W}/(\text{K m})] = 301.8 \pm 1.5 + (-40.32 \pm 18)/(1 + (-0.0129 \pm 0.003)T/[K])$$

$$\bar{c}_{Au}/[\text{J}/(\text{kg K})] = 129 \pm 1.5$$

$$\rho_{Au}/[\text{kg/m}^3] = 19320$$

$$k_K/[\text{W}/(\text{K m})] = (5.24 \pm 0.32) \times 10^{-3}(T/[K])^{1.02\pm0.02}$$

$$\bar{c}_K/[\text{J}/(\text{kg K})] = (1.65 \pm 0.2) \times 10^2 + (2.85 \pm 0.2)T/[K] - (2.87 \pm 0.4) \times 10^{-3}T^2/[K^2]$$

$$\rho_K/[\text{kg/m}^3] = 1420$$

Results

The electric current density in the gold thin film shows pronounced variations due to the presence of holes. The temperature is, however, almost constant due to the high thermal conductivity of the system and the periodic boundary conditions (Fig. S7 and Fig. S8). The maximum temperature depends on the free parameter h, chosen here to match the experimental curves. The temperature rises monotonically as a function of time and calculations are stopped arbitrarily at time $t = 1$ s, near steady state. A plot of the maximum temperature vs. applied voltage is shown in Fig. S9.
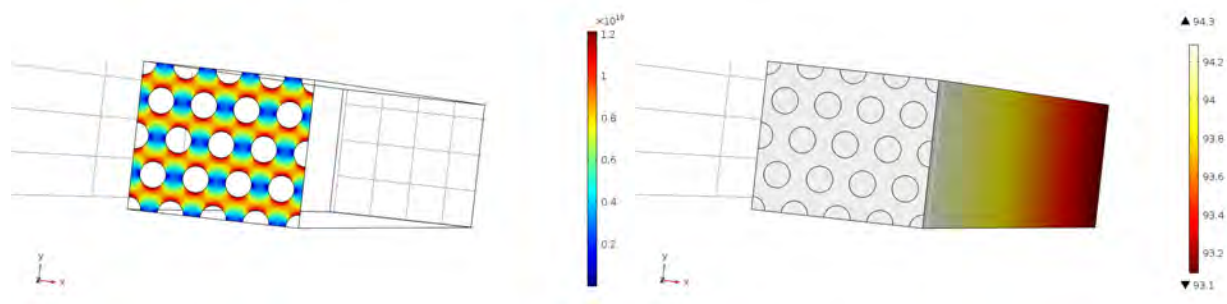
Figure S7: Left: current density (in A/m^2). Right: Temperature (in °C). Both calculations are for a system with 600 nm diameter holes and a 40 nm thickness for the gold layer at $V_a = 2.35$ V.
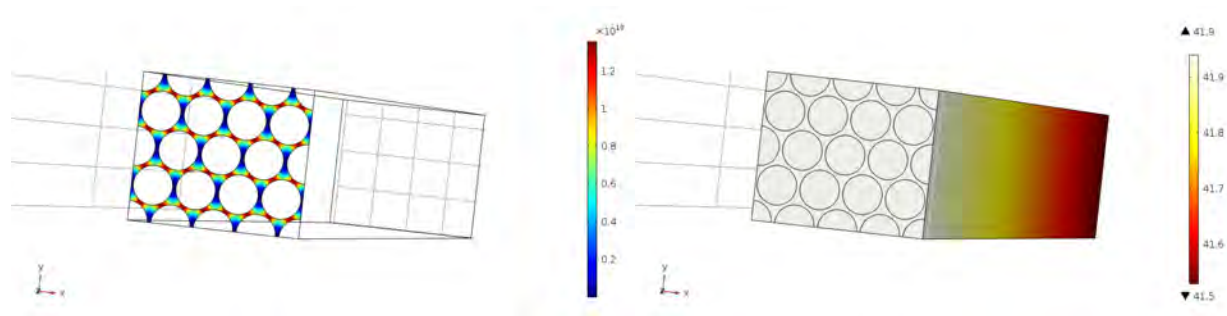
Figure S8: Left: current density (in A/m^2). Right: Temperature (in °C). Both calculations are for a system with 900 nm diameter holes and a 40 nm thickness for the gold layer at $V_a = 2.35$ V.

The computed temperature versus voltage curves follow a quadratic shape, as expected for the Joule dissipation of an ohmic element. The result depends on the flux boundary conditions, and thus on the h parameter, that could also vary with temperature, but was considered here constant. The periodic calculation is the basis for an equivalent model of the macroscopic sample, for which small geometrical details can not be assessed.

Large sample extension

In the case of a large sample, effective parameters must be used to take into account the presence of holes in the gold thin film. The mass density can be easily scaled by the volume
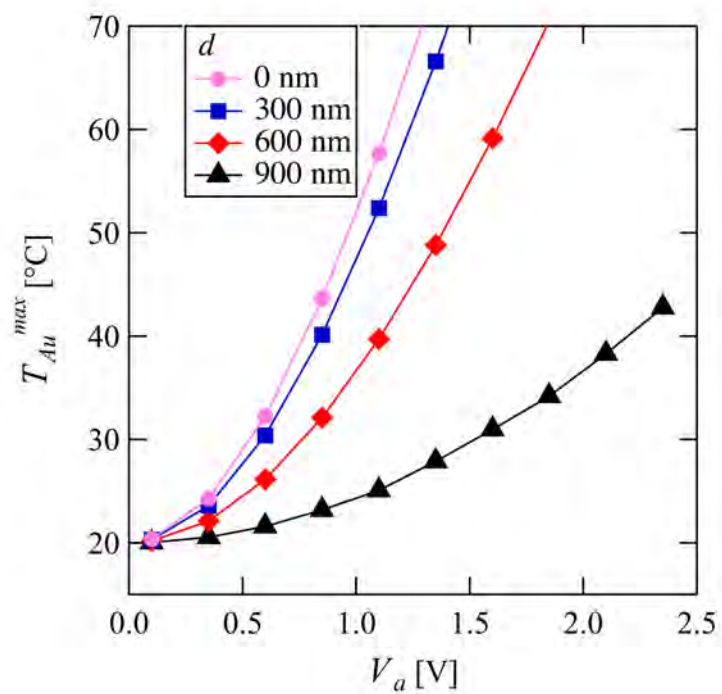
Figure S9: Numerical results of the maximum temperature on the gold side of the Kapton tape as a function of the applied voltage V_a, for indicated hole diameters, at $t = 1$ s. The thickness of the gold layer is 40 nm.

filling. The electrical and heat conductivities must also be modified by geometric factors. To determine the geometrical dependence of the heat conductivity κ, two sides of the holey gold thin film considered previously were put at fixed temperatures with a difference of 0.1 K, namely $T(x = 0) = 20.1\,°C$ and $T(x = L) = 20\,°C$, keeping the periodic conditions in the y direction. The heat flux $\boldsymbol{q} = -\kappa \nabla T$ was then numerically calculated in the steady state condition and integrated for the boundary $x = L$ to obtain the heat current $H_c = \int_{x=L} \boldsymbol{q} \cdot d\boldsymbol{S}$.
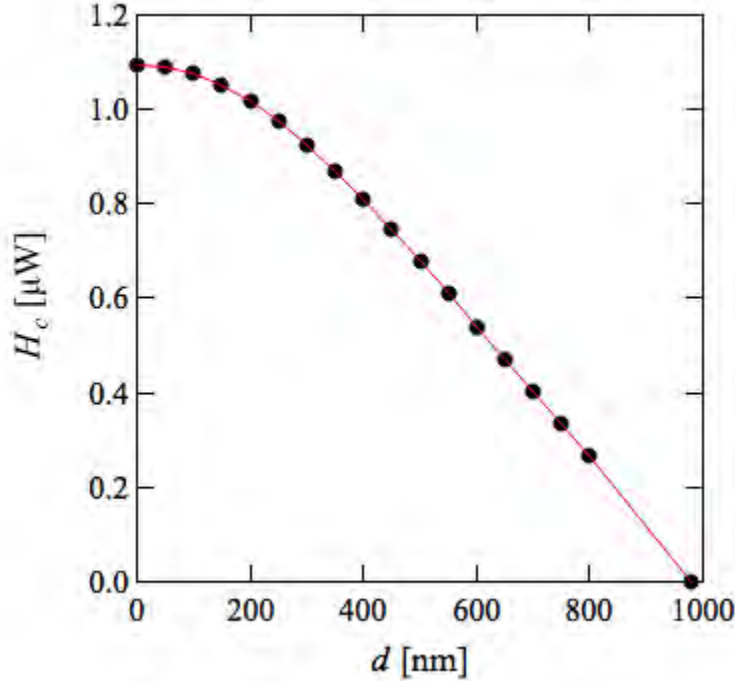
Figure S10: Heat current computed for different hole diameters (black symbols) and fit with quadratic-linear function (red curve) $H_c = a_1(1 - a_2 d^2/(1 + d a_3))$, where H_c is the heat current and d is the hole diameter, with parameters $a_1 = 1.0957 \times 10^{-6}$ W (given), $a_2 = 2.7602 \times 10^{12} \pm 8.9 \times 10^{10}$ m^{-2} and $a_3 = 1.658 \times 10^6 \pm 9.7 \times 10^4$ m^{-1}.

We deduce from Fig. S10 that the geometrical factor for the in-plane thermal conductivity is $f_c = 1 - a_2 d^2/(1 + d a_3)$, with $a_2 = 2.7602 \times 10^{12}$ m^{-2} and $a_3 = 1.658 \times 10^6$ m^{-1}. The same factor is valid for the in-plane electrical conductivity $\sigma^p = 1/\rho^p_{eAu}$, as the heat flow $\boldsymbol{q}$ and the electric current $\boldsymbol{j}$ satisfy the same equation in steady state conditions with non-conducting boundaries, namely $\nabla \cdot \boldsymbol{j} = 0$ and $\nabla \cdot \boldsymbol{q} = 0$.

The mass density is modified by the volume fraction. In a triangular lattice the unit cell

has an area of $\sqrt{3}a/2$, therefore the volume fraction is $f_v = 1 - 2\pi(d/2)^2/\sqrt{3}a^2$. This factor modifies also the out-of-plane thermal conductivity κ_{Au}^s. In summary, we obtain:

$$\kappa_{Au}^p = \kappa_{Au} f_c, \tag{2}$$

$$\kappa_{Au}^s = \kappa_{Au} f_v, \tag{3}$$

$$\rho_{Au}^{eff} = \rho_{Au} f_v, \tag{4}$$

$$\rho_{eAu}^p = \rho_{eAu}/f_c. \tag{5}$$

Steady-state temperature of the system: h_{eff}

The temperature evolution of the system under a constant current I heating can be analysed as follows. First, we neglect the vertical variations of temperature in the metal film, and consider only the convective heat lost at the top and bottom boundaries. Then the temperature gradients can be neglected and the convective heat loss can be directly incorporated into the heat equation as:

$$\rho\bar{c}\frac{\partial T}{\partial t} = \boldsymbol{j} \cdot \boldsymbol{E} - h_{eff}(T - T_0)/t_h, \tag{6}$$

where h_{eff} is the effective convective heat loss parameter. At equilibrium, the time derivative of the temperature is zero, and the equilibrium temperature T_{eq} can be found algebraically by solving:

$$\boldsymbol{j} \cdot \boldsymbol{E} = h_{eff}(T_{eq} - T_0)/t_h. \tag{7}$$

Let's consider first the case of total constant current I heating. Given the cross section A of the sample, Eq. (7) can be written as:

$$\rho^p_{eAu}\frac{I^2}{A^2} = h_{eff}(T_{eq} - T_0)/t_h, \tag{8}$$

$$\frac{\rho_{eAu}}{f_c}\frac{I^2}{A^2} = h_{eff}(T_{eq} - T_0)/t_h, \tag{9}$$

$$\rho_{eAu} = \frac{f_c h_{eff} A^2}{t_h I^2}(T_{eq} - T_0). \tag{10}$$

Then we use the parametrization of the resistivity $\rho_{eAu}(T) = u_0 + u_1 T$ (see Subsection **Physical parameters**):

$$u_0 + u_1 T_{eq} = \frac{f_c h_{eff} A^2}{t_h I^2}(T_{eq} - T_0). \tag{11}$$

Let's call $v = \frac{f_c h_{eff} A^2}{t_h I^2}$, then:

$$T_{eq} = \frac{u_0 + vT_0}{v - u_1}, \tag{12}$$

$$T_{eq} = \frac{\frac{u_0 t_h I^2}{f_c h_{eff} A^2} + T_0}{1 - \frac{u_1 t_h I^2}{f_c h_{eff} A^2}}. \tag{13}$$

In the case of constant voltage V_a heating, for a sample of length L, we get the following equation from Eq. (7):

$$0 = u_1 T_{eq}^2 + (u_0 - u_1 T_0)T_{eq} - u_0 T_0 - \frac{V_a^2}{L^2}\frac{t_h f_c}{h_{eff}}. \tag{14}$$

By calling $r = u_0 T_0 + \frac{V_a^2}{L^2}\frac{t_h f_c}{h_{eff}}$, we get:

$$T_e = \frac{(-u_0 + uT_0)}{2u} + \frac{\sqrt{(u_0 - uT_0)^2 + 4ur}}{2u}. \tag{15}$$

The following factors h_{eff}, f_c, u_0 and u_1 are assumed independent of d and T and an

estimate for h_{eff} at fixed t_h can be obtained. By using Eqs. (13) and (15), the steady-state temperatures for each d can be inferred by taking *ad hoc* values $h_{eff} = 2h = 500$ W/(m²K) (Figure S11, panels (a) and (b)) and $h_{eff} = 2h = 200$ W/(m²K) (Figure S11, panels (c) and (d)) as well as the experimental values for the sample width and length.

We experimentally determined the steady-state temperature as a function of the applied bias in the fabricated patches. In Fig. S12, the result for the unpatterned sample ($d = 0$ nm) is shown. The resistivity of the Ti/Au thin layer was measured as a function of the temperature: $\rho^{exp}(T) = u_0^{exp} + u_1^{exp}T$, with $u_0^{exp} = 1.515 \times 10^{-08} \pm 2 \times 10^{-10}$ Ω m and $u_1^{exp} = 1.316 \times 10^{-10} \pm 7 \times 10^{-13}$ Ω m/K. Accordingly, by fitting the Eq. (15) to the data of Fig. S12, we estimate $h = 91.6 \pm 0.3$ W/(m²/K).

Macroscopic model

By placing the above effective parameters in a three-dimensional model, we can obtain the temperature distribution in the patch as shown in Fig. S13. It consists of a Kapton disc with the central area covered with the heating gold thin film, with thicker gold areas in the borders, and two contacts in these borders, to account for the heat flow into the external leads.

The maximum temperature T_{Au}^{max} is attained at the center of the system. This temperature was calculated for different hole diameters d, that can be seen in Fig. S12, and also for different t_h film thicknesses. The total electric current was also calculated and it is shown in Fig. S13. Very high electrical current values are obtained for small holes, especially on thin films thicker than 75 nm, far from typical consumer power supplies. That would require in particular thick electrical power leads. Such electrical power leads are incompatible with the Kapton disc dimensions.

From Fig. S14 and Fig. S15, two sets of parameters were chosen, $S1 : \{d = 320$ nm$, t_h = 40$ nm$\}$ and $S2 : \{d = 850$ nm$, t_h = 100$ nm$\}$, and the realistic application of the patch
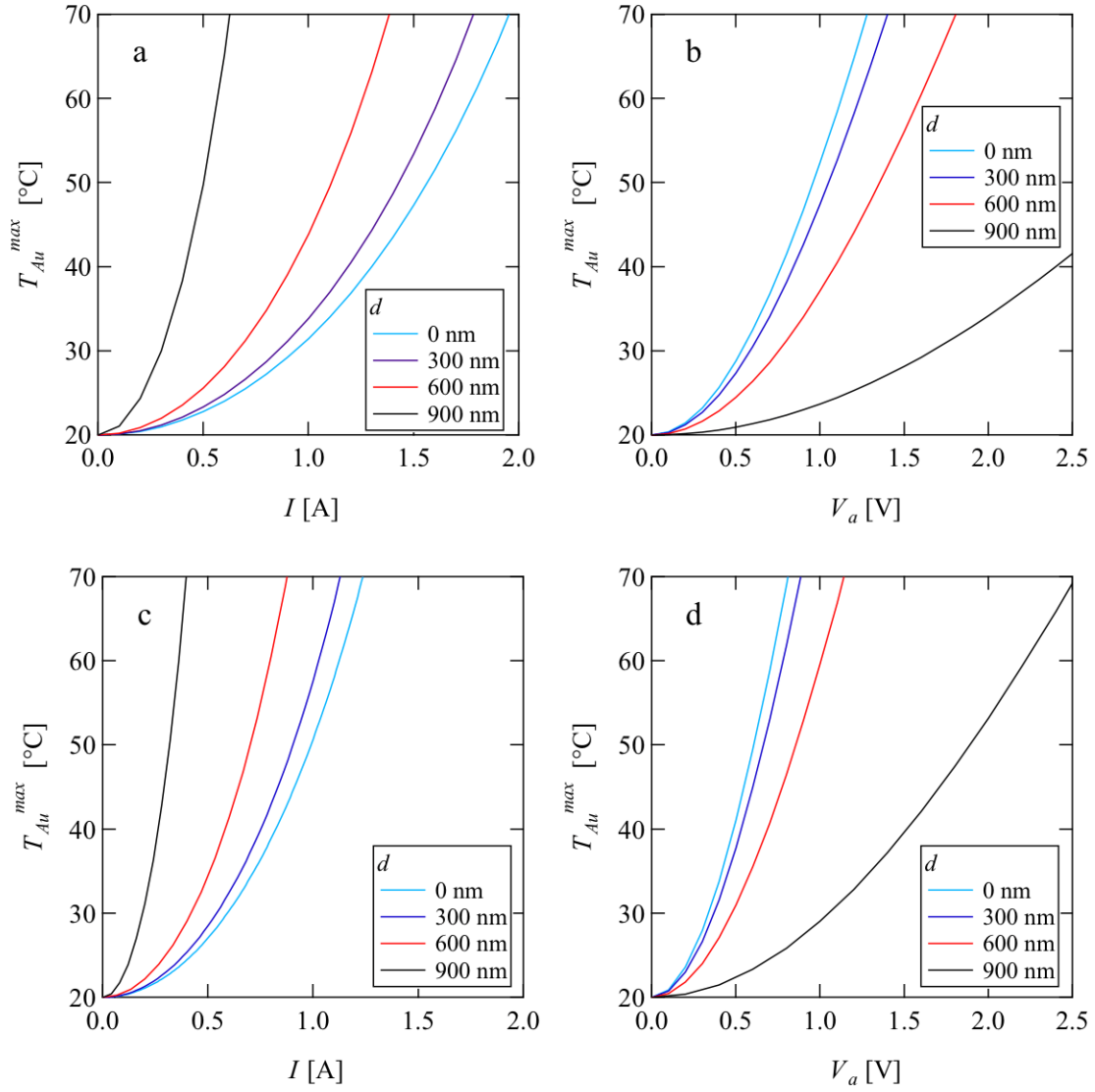
Figure S11: Calculated steady-state temperature T_{Au}^{max} as a function of constant current I and applied bias V_a, respectively, at indicated d for (a, b) $h_{eff} = 2h = 500$ W/(m²K) and (c,d) $h_{eff} = 2h = 200$ W/(m²K).
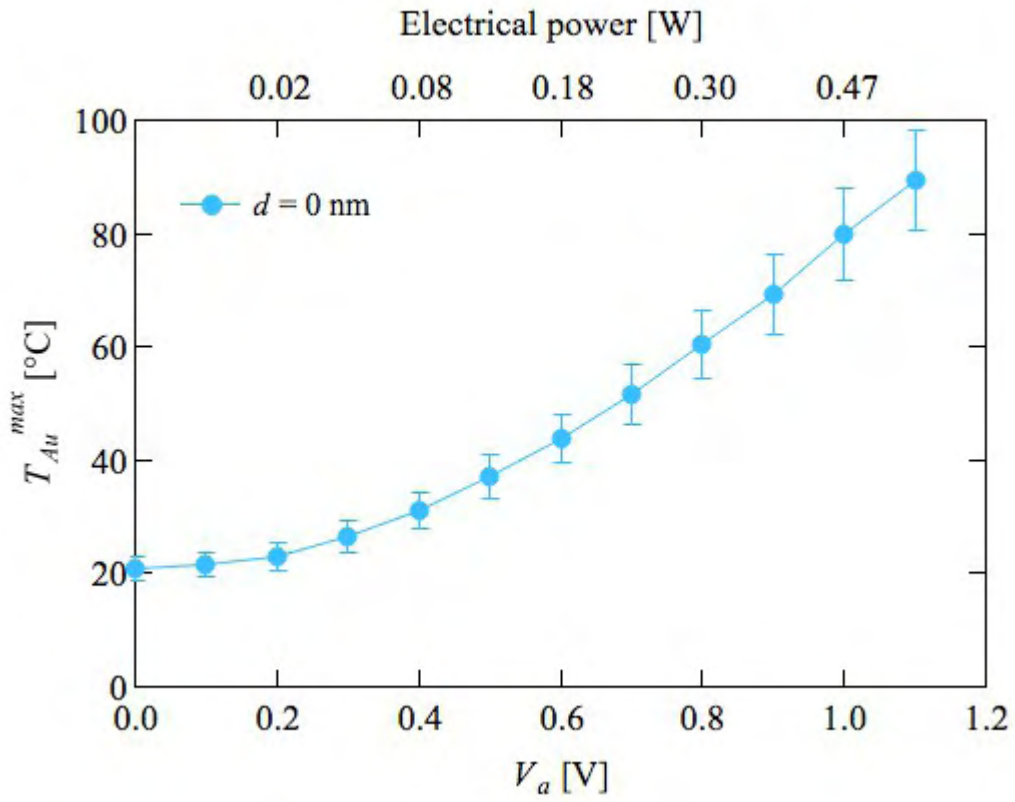
Figure S12: The experimentally determined dependence of the steady-state temperature T_{Au}^{max} as a function of the applied bias V_a for the unpatterned sample.
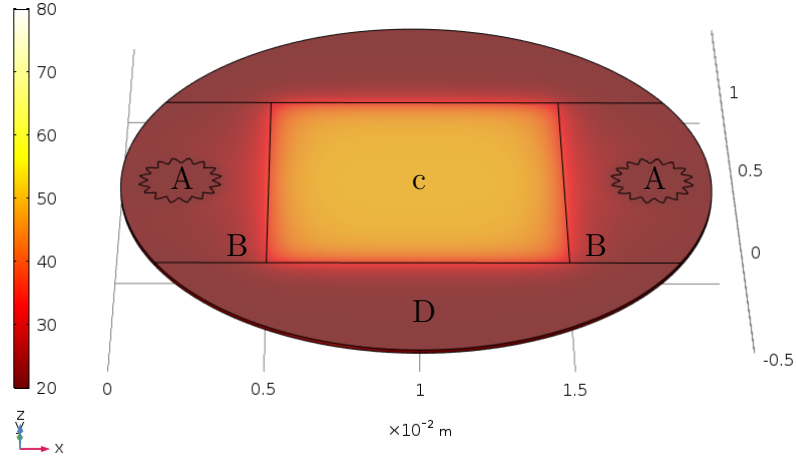
Figure S13: Top face temperature distribution of the patch (in °C) after 60 s with 1.5 V bias applied in contacts A. The heating gold film c has $h = 250$ W/(m²K) on all parts, except on contacts A where $h = 10000$ W/(m²K). Here $T_{ref} = 20$ °C. Dimensions of the Kapton disc D are 1 cm radius and 0.125 mm thickness. The heating gold film c is 100 nm thick, has 850 nm holes, and measures 1 cm × 1 cm. The lateral contact gold areas B are 2 times thicker than the central area $(t_c = 2t_h)$, i.e. 80 nm, and have 1 cm width. The contacts A are 2.5 mm diameter with ripples for enhanced mechanical properties. The parametrization for the contacts A border is $(x, y)=((0.00125+0.00015\cos(10s\text{-}\pi))\cos(s), (0.00125+0.00015\cos(10s\text{-}\pi))\sin(s))$, with s between 0 and 2π. The center-to-center separation of contacts A is 16 mm.
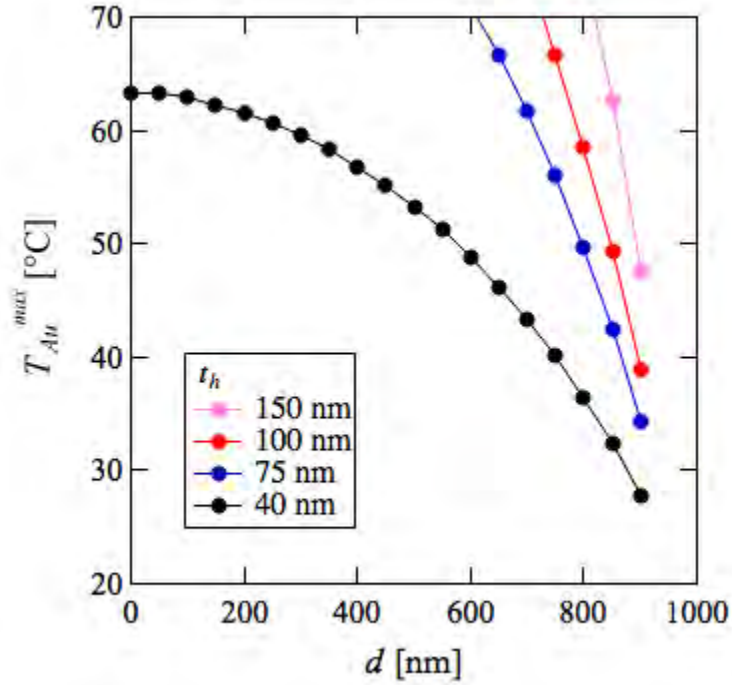
Figure S14: Maximum top face temperature T_{Au}^{max} as a function of the hole diameter for different thicknesses of the heating film at $V_a = 1.5$ V applied voltage.

was considered. Through holes at the contacts A (Fig. S11) filled with conductive epoxy EPO TEK® H20E were considered as macroscopic electrical contacts. Due to their small dimensions, the electrically conducting elements of the patch were included in the COMSOL model as a shell of zero thickness with corresponding electrical and thermal properties. An epidermis layer of 60 μm with a dermis layer of 500 μm[S6] have been taken into account, in
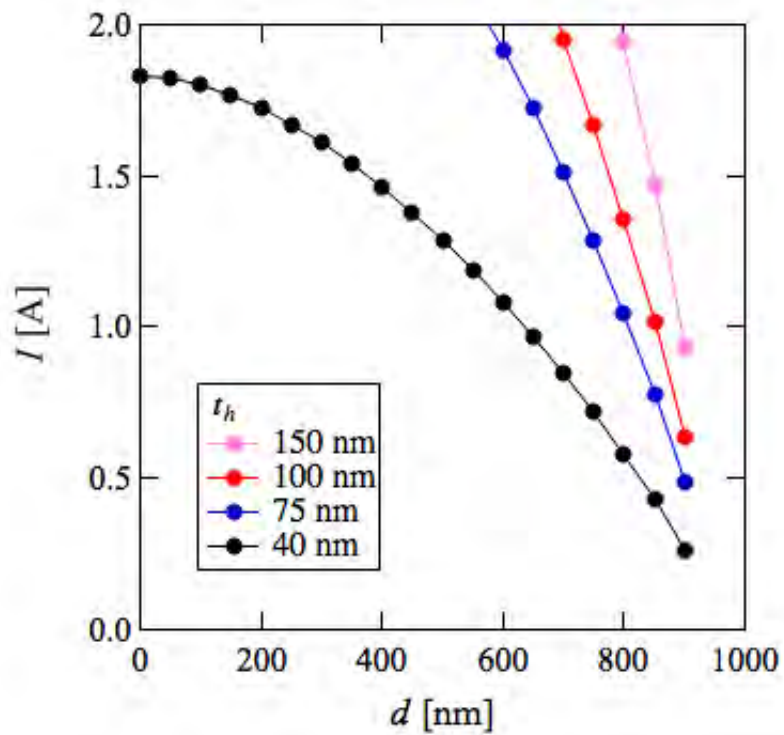
Figure S15: Electrical current in the patch as a function of the hole diameter for different thicknesses of the heating gold film at $V_a = 1.5$ V applied voltage.

perfect thermal contact with the heating side of the disc, with physical properties[S6,S7]:

$$k_{\text{H20E}}/[\text{W}/(\text{m K})] = 29$$

$$\bar{c}_{\text{H20E}}/[\text{J}/(\text{kg K})] = 233, \qquad \text{using silver heat capacity}$$

$$\rho_{\text{H20E}}/[\text{kg}/\text{m}^3] = 2600$$

$$k_{epidermis}/[\text{W}/(\text{m K})] = 0.26$$

$$\bar{c}_{epidermis}/[\text{J}/(\text{kg K})] = 3600$$

$$\rho_{epidermis}/[\text{kg}/\text{m}^3] = 1200$$

$$k_{dermis}/[\text{W}/(\text{m K})] = 0.53$$

$$\bar{c}_{dermis}/[\text{J}/(\text{kg K})] = 3600$$

$$\rho_{dermis}/[\text{kg}/\text{m}^3] = 1200.$$

For the dermis, four heat transfer parameters were considered, namely $h_b = 10, 10^2, 10^3, 10^4$ W/(m²K), with $T_{ref} = 36.5\,°\text{C}$. On the top external face of the Kapton, a heat transfer parameter of 250 W/(m²K), and $T_{ref} = 20\,°\text{C}$ were used, while on the E20H EPO TEK contacts a heat transfer parameter of 10^4 W/(m²K), and $T_{ref} = 20\,°\text{C}$ were taken. Initial temperature was 36.5 °C everywhere.
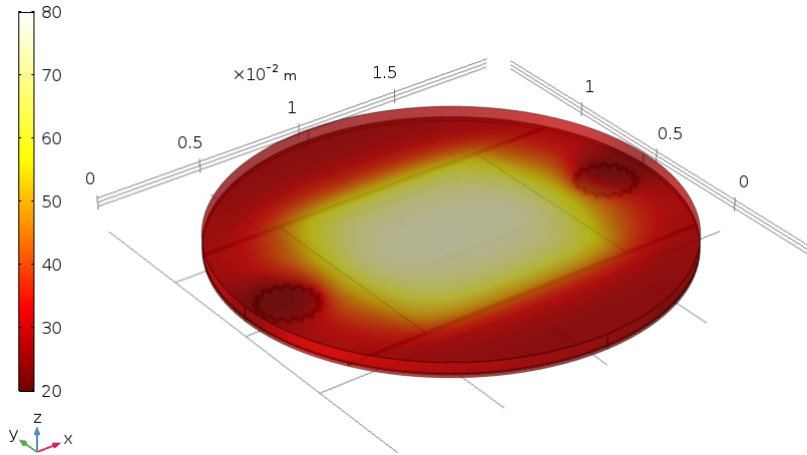
Figure S16: Temperature distribution (in °C) within the heating device attached to the skin [$d = 320$ nm, $t_h = 40$ nm, 60 s time, and $h_b = 100$ W/(m²K) with 1.5 V applied bias].

The temperature as a function of the depth in the skin, for a line passing through the

axis of the system between 0 and 560 μm, *i.e.* center of the tape in the direction of skin, can be seen in Fig. S17 (set $S1$) and Fig. S18 (Set $S2$) for different values of h_b.
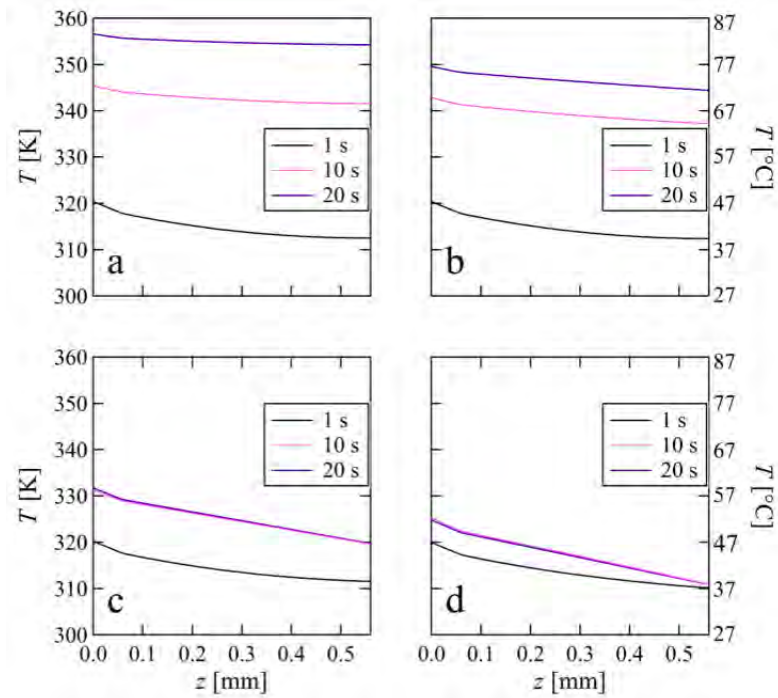
Figure S17: $S1$. (a) Temperature distribution inside the skin layer with $h_b = 10$ W/(m^{2}K) at different indicated times. (b) Temperature distribution inside the skin layer with $h_b = 10^2$ W/(m^{2}K) at different indicated times. (c) Temperature distribution inside the skin layer with $h_b = 10^3$ W/(m^{2}K) at different indicated times. (d) Temperature distribution inside the skin layer with $h_b = 10^4$ W/(m^{2}K) at different indicated times.
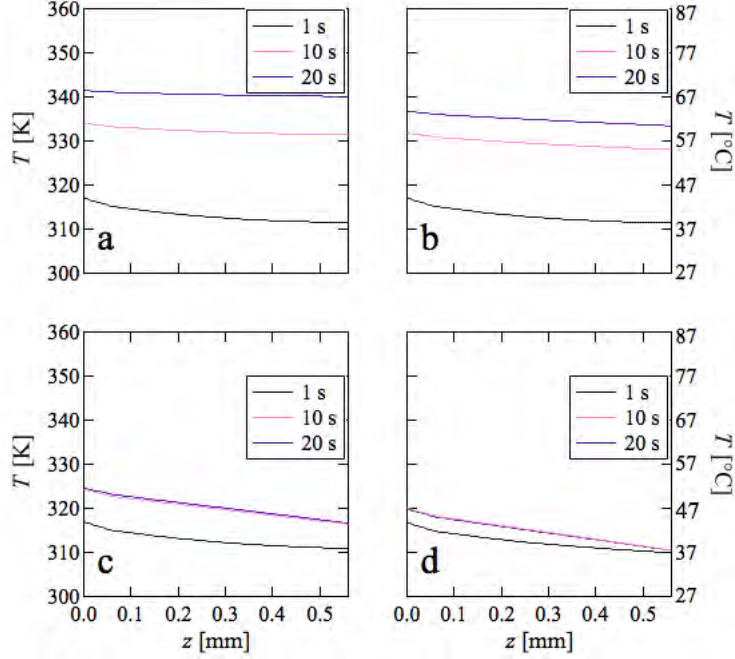
Figure S18: *S*2. (a) Temperature distribution inside the skin layer with $h_b = 10$ W/(m²K) at different indicated times. (b) Temperature distribution inside the skin layer with $h_b = 10^2$ W/(m²K) at different indicated times. (c) Temperature distribution inside the skin layer with $h_b = 10^3$ W/(m²K) at different indicated times. (d) Temperature distribution inside the skin layer with $h_b = 10^4$ W/(m²K) at different indicated times.

Copper back contact devices

Two copper back contacts of 3.5 mm × 3.5 mm centered at the star shaped through contacts were added in the calculation to the electrothermal system considered in the previous section. The nano-patterned area is now 11 mm × 11 mm. The thickness of the Kapton is 75 μm, and the thickness of the copper layer is 70 μm. The geometry is depicted in Fig. S19. All other parameters are kept the same.
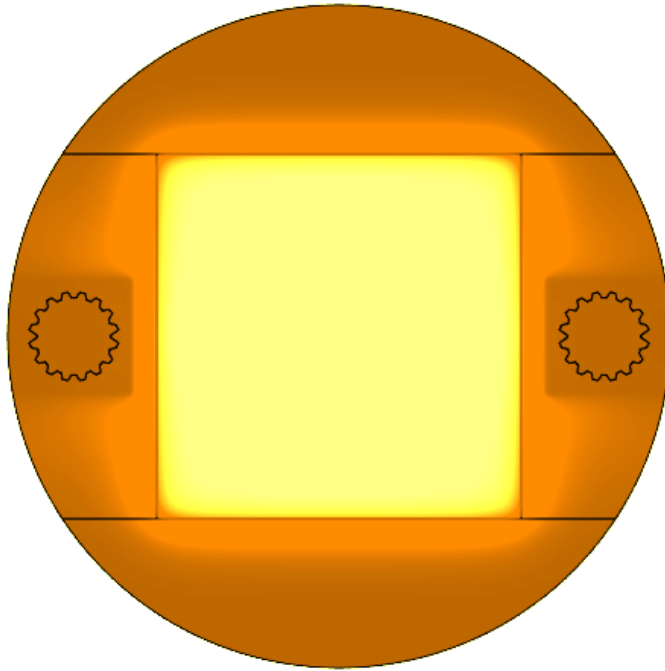
Figure S19: Device with added rectangular copper contacts on the Kapton back side and in contact with the filling epoxy. The distance between the two horizontal black lines is 11 mm (scale bar).

The performance of the new electrothermal system is shown in Fig. S20:
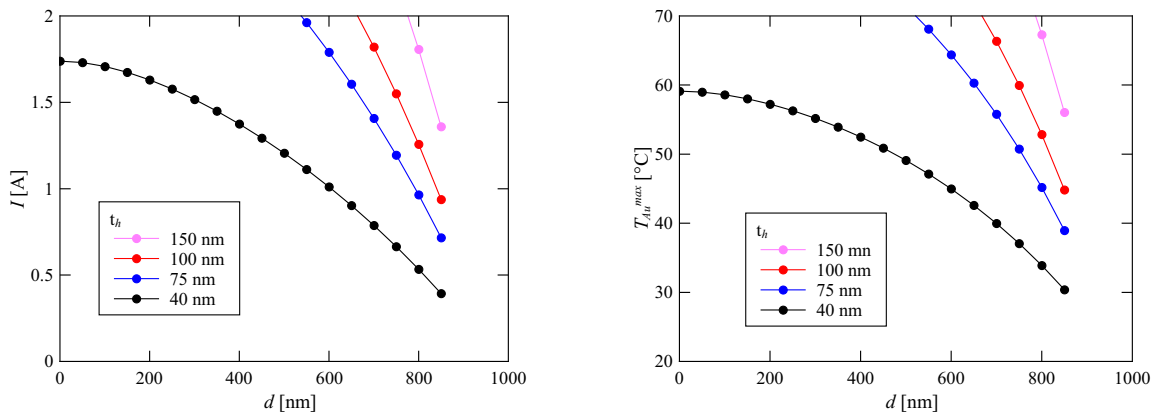
Figure S20: Left: Total electrical current in the patch vs hole diameter at constant bias 1.5 V. Right: Maximum top face temperature T_{Au}^{max} as a function of the hole diameter for different thicknesses of the heating film at $V_a = 1.5$ V applied voltage. These two quantities were calculated at 60 s heating time.

The behaviour of the device on the skin is shown in Fig. S21, using the set $S1 : \{d = 320 \text{ nm}, t_h = 40 \text{ nm}\}$.
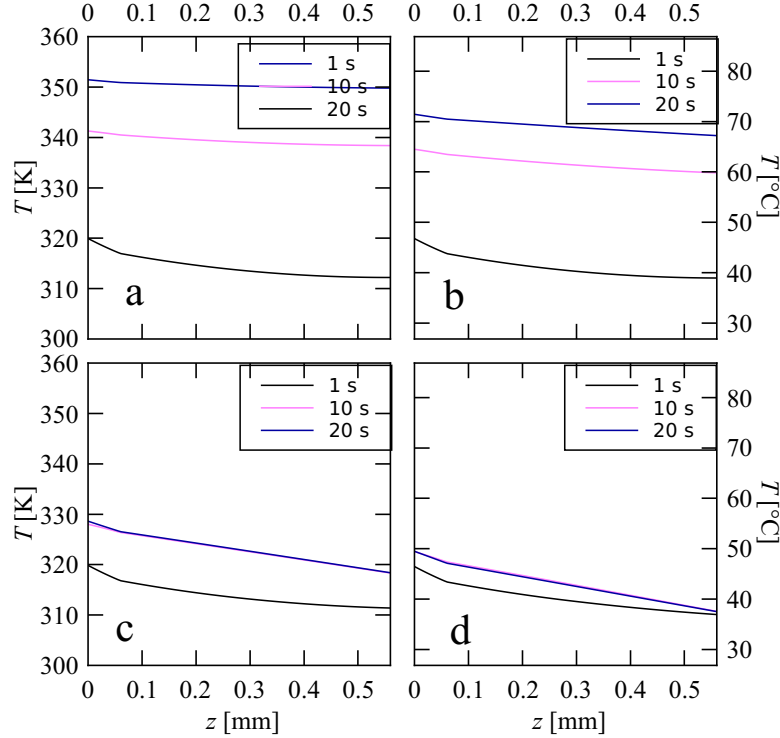
Figure S21: $S1$ with copper back contacts. (a) Temperature distribution inside the skin layer with $h_b = 10 \text{ W}/(\text{m}^2\text{K})$ at different indicated times. (b) Temperature distribution inside the skin layer with $h_b = 10^2 \text{ W}/(\text{m}^2\text{K})$ at different indicated times. (c) Temperature distribution inside the skin layer with $h_b = 10^3 \text{ W}/(\text{m}^2\text{K})$ at different indicated times. (d) Temperature distribution inside the skin layer with $h_b = 10^4 \text{ W}/(\text{m}^2\text{K})$ at different indicated times.

The behaviour is qualitatively similar to the devices without copper back contacts, with temperature profiles evolving slightly below the simpler design devices.

The electrical resistance of the gold thin films without holes is negligible, so very high electrical currents result when an electrical bias is applied. In a practical system, this is a nuisance as it would require high power electrical cords and supplies. The presence of holes increases the electrical resistance of the gold thin film and decreases the electrical current. This electrical current can not be very low as it would decrease in turn the Joule dissipation. As a simple rule, electrical currents of 1 A at voltages of 1 V will result in 1 W

of electrical power dissipation. This level of dissipation can easily heat small circuit elements to temperatures of 100 °C under typical thermal resistances encountered in electronic circuit boards. This is true for the electrothermal patches considered here. Concerning the heating of the skin, the heat transfer parameter of the deeper skin is not known precisely, therefore, several values were tried. At low h_b values, 10 or 100 W/(m^{2}K), the temperature profile changes fast in a time window of 10 s, with temperatures situated above 55 °C. For high values of $h_b = 10^4$ W/(m^{2}K), the temperature in the deeper dermis stays constant and a uniform gradient develops, meaning that heat is transferred at a constant rate. The temperature profile settles in a time window of 10 s. Any imperfections in the thermal contact between the patch and the skin will lead to a lower heat transfer towards the skin. Humidity of the skin could also lead to some electrical current loss, depending on the ion content of the water. To minimize this effect, pre-cleaning followed by the application of a non-aqueous isolating layer on the skin before contact with the patch would likely be beneficial.

Calculations were performed to obtain the effect of patterned holes in a heating gold thin film deposited on a structured Kapton disc. From these calculations, hole diameters and film thicknesses were chosen such as to produce temperatures around 50 °C without using very high electrical currents for heating. Results were also obtained for the temperature distribution in the skin for different heat transfer parameters.

Electrothermal insulin delivery
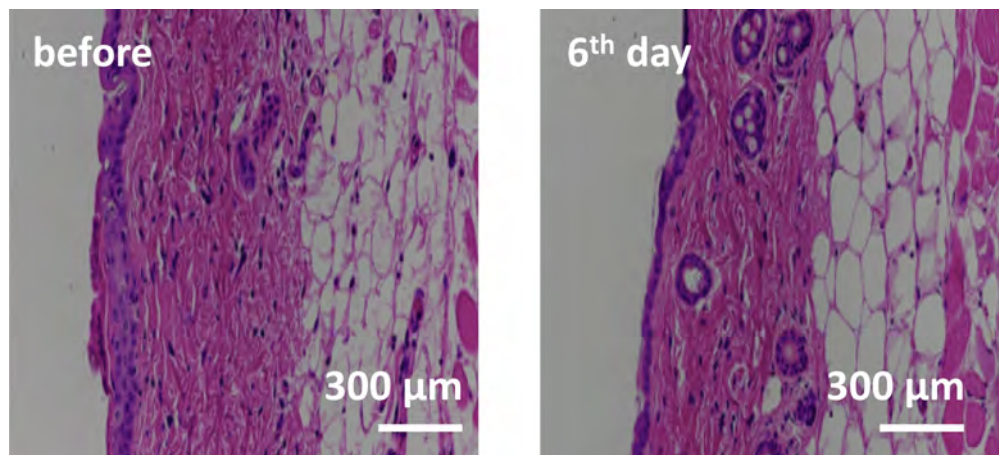
Figure S22: Hematoxylin and eosin staining of mice skin before (left panel) and after (right panel) stimulation every day for 10 min at 52 °C.
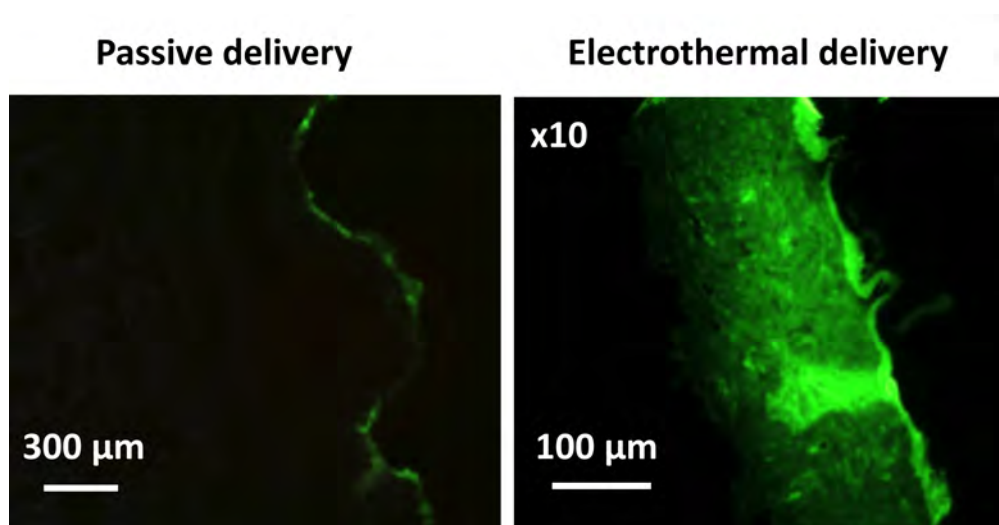
Figure S23: *In vitro* cumulative permeation (2 h) of FITC-insulin delivered from an electrothermal patch loaded with 100 μg (2.8 IU) insulin across mouse skin upon continuous application of 1.0 V bias voltage for 10 min (right panel) as well as passive delivery (left panel).

List of abbreviations

x, y, z	:coordinates in cartesian coordinate system	ρ_{Au} :	mass density of gold
ρ	:mass density	ρ_{eAu} :	electrical resistivity of gold
ρ_e	:electrical resitivity	κ_{Au} :	heat conductivity of gold
$\bar{c}$	:unit mass heat capacity	c_{Au} :	unit mass heat capacity of gold
κ	:heat conductivity	ρ_K :	mass density of Kapton
T	:temperature	κ_K :	heat conductivity of Kapton
$\boldsymbol{j}$	:electric current density	c_K :	unit mass heat capacity of Kapton
$\boldsymbol{E}$	:electric field	f_c :	geometrical factor effective conductivity
ϕ	:electric potential	f_v :	geometrical factor effective volume
T_{ref}	:reference temperature of environment	$\boldsymbol{q}$:	heat flow
h	:heat transfer parameter	κ_{Au}^p :	effective in plane κ of holey gold film
σ	:electrical conductivity	κ_{Au}^s :	effective out of plane κ of holey gold film
$\hat{n}$	:external normal to boundary	ρ_{eAu}^p :	effective in plane ρ_e of holey gold film
t_K	:thickness of Kapton tape	ρ_{Au}^{eff} :	effective ρ of holey gold film
t_h	:thickness of holey gold film	H_c :	heat current, $\boldsymbol{q}$ integrated on surface
t_c	:thickness of lateral gold contacts	I_c :	electrical current, $\boldsymbol{j}$ integrated on surface
L	:length of periodic section along x axis	$\rho_x, \rho_{ex}, c_x, \kappa_x$:	ρ, ρ_e, c, κ of x substance, respectively
w	:length of periodic section along y axis	V_a :	applied bias
d	:holes diameter	t :	time
a	:separation between holes in the triangular lattice	$\boldsymbol{S}$:	surface
rGO	:reduced graphene oxide	HPLc :	High-performance liquid chromatography
ELISA	:enzyme-linked immunosorbent assay	NH :	nanohole

References

(S1) F. John, *Partial Differential Equations*, Springer-Verlag, New York, 1982.

(S2) R.A. Matula, *Electrical Resistivity of Copper, Gold, Palladium, and Silver*, Journal of Physical and Chemical Reference Data **8**, 1147 (1979).

(S3) R.W. Powell, C.Y. Ho, P.E. Liley, *Thermal Conductivity of Selected Materials*, NSRDS-NBS-8, 1966.

(S4) D.J. Benford, T.J. Powers, S.H. Moseley, *Thermal Conductivity of Kapton Tape*, Cryogenics **39**, 93 (1999).

(S5) NIST Materials Property Database, `http://cryogenics.nist.gov/MPropsMAY/PolyimideKapton/PolyimideKapton_rev.htm`. The specific heat extrapolated from given fit above 300 K.

(S6) T. Dai, B.M. Pikkula, L.V. Wang, B. Anvari, *Comparison of Human Skin Opto-thermal Response to Near-infrared and Visible Laser Irradiations: A Theoretical Investigation*, Phys Med Biol **49**, 4861 (2004).

(S7) `http://www.epotek.com/site/administrator/components/com_products/assets/files/Style_Uploads/H20E.pdf`